Thermal shock behavior of Ti$_3$AlC$_2$ from between 200 °C and 1300 °C

Y.W. Bao, X.H. Wang, H.B. Zhang, Y.C. Zhou*

Shenyang National Laboratory for Materials Science, Institute of Metal Research, Chinese Academy of Sciences, 72 Wenhua Road, Shenyang 110016, PR China

Abstract

The retained strength and hardness of Ti$_3$AlC$_2$ bars quenched from 200 to 1300 °C in air, water and silicon oil were investigated to probe the thermal shock resistance of Ti$_3$AlC$_2$ in various media. The measured retained strength displayed different trends for the samples quenched in various media. For the samples quenched in air, the retained strength showed somewhat enhancement with increase of the temperature difference. For the samples quenched in water, the retained strength exhibited a complex evolution and could be divided into four zones, i.e., (i) no damage zone (20–300 °C), (ii) strength degradation zone (300–500 °C), (iii) stable strength zone (500–1000 °C), and (iv) strength enhancement zone (1000–1300 °C). Therefore, the minimum retained strength in the third zone, which is higher than 60% of the initial strength, provided a prediction that the strength loss by thermal shock for Ti$_3$AlC$_2$ should be less than 40%. SEM analysis revealed that an oxide scale of α-Al$_2$O$_3$ was formed at high temperature for which the residual stress was calculated. The strength degradation in the second temperature zone was imputed to the weakening of grain boundaries caused by water infiltration, whereas the strength enhancements for the air-quenched samples in the fourth zone was attributed to the formation of oxide scale and the residual compressive stresses in the oxide layer. The damage caused by quenching in oil for this ceramic was demonstrated between that of air and water quenching. Finite element method (FEM) was used to simulate the failure in bending, and the results indicated that the strength of the sample with an oxide scale was about 5–10% higher than that of homogeneous sample.
© 2004 Elsevier Ltd. All rights reserved.

Keywords: Thermal shock; Retained strength; Ti$_3$AlC$_2$; Oxidation

1. Introduction

As an important layered ternary ceramic and a promising candidate for high temperature application, Ti$_3$AlC$_2$ has attracted growing attentions during the past decade.[1–6] It displays high elastic modulus, low hardness, high fracture toughness and strength, metallic conductivity, good oxidation resistance and machinability.[3–6] Moreover, Hertzian indentation tests showed that Ti$_3$AlC$_2$ as well as other layered ternary ceramics was typical quasi-plastic materials with high damage tolerance and low shear resistance.[7,8]

The capacity to resist rapid temperature change is an essential property for ceramics used at high temperatures.[9–11] When a component is subjected to a rapid temperature-drop, transient tensile stresses are generated in the surface layer due to the instantaneous temperature difference between the surface layer and the inner body. The temperature difference corresponding to the damage initiation, ΔT_c, therefore, has been widely used as a thermal shock resistance factor.[9–12]

$$R = \frac{\sigma_f(1-\nu)}{\alpha E} \qquad (1)$$

where σ_f is the strength, α is the thermal expansion coefficient, E is the elastic modulus and ν is Poisson's ratio. For brittle materials, crack initiation and growth need not

* Corresponding author. Tel.: +86 24 23971762; fax: +86 24 23891320.
  E-mail address: yczhou@imr.ac.cn (Y.C. Zhou).

only a certain time but also a certain area of the applied stress.[13] Due to the high stress gradient normal to the surface and the short duration of the thermal shock stress, the critical temperature is often higher than the estimation from Eq. (1). Kim[14] and Sherman and Schlumm[15] have revealed that the thermal shock resistance of a ceramic is strongly affected by factors that govern the gradient and the duration of the thermal stresses, such as the heat conductivity, the geometric shape and size of the sample. Many modifications in the calculation of thermal shock resistance have been well-established,[9,11,12,16] which provide more accurate prediction of the critical temperature for damage initiation.

Quenching-strength test is a common laboratory approach to evaluate the thermal shock resistance of ceramics[11] because the strength degradation reflects thermal damage of a material. Different quenching media may lead to dissimilar damages. Among them, water causes the most rapid cooling, and consequently, is an appropriate choice for evaluating the thermal shock behavior of a material with high thermal shock resistance.[11,12] Air is a real medium for many practical applications, so quenching in air is important for simulating environmental load. In general, the thermal shock damage of ceramics increases with increasing temperature difference, and the retained strength drops abruptly at the critical temperature[16–18] because of the crack-sensitivity of ceramics. However, for the layered Ti$_3$AlC$_2$ quenched in water, an interesting phenomenon has been noticed by Tzenov and Barsoum[1] and Wang and Zhou[4] respectively, i.e., the retained strength increased with increasing temperature difference in a certain temperature range. This result is contradictory to the prediction based on the conventional damage mechanics and thermomechanics. Since previous tests were limited in sample numbers and temperature range, many important issues such as the critical temperature for thermal shock damage, the mechanism of the abnormal thermal shock resistance and the effects of the quenching media are unclear to date. Obviously, it is significant to explore the causes for above questions.

This work focuses on a systematic investigation of the thermal shock behavior of Ti$_3$AlC$_2$ over a large temperature range and of the critical temperature for strength degradation, by quenching in water, in air and in oil, respectively. The emphases are placed on three aspects: (i) difference in thermal shock damage between quenching in water, air and oil; (ii) explanations for the abnormal thermal shock behavior of Ti$_3$AlC$_2$; and (iii) evidences for the explanations based on SEM observation, theoretical calculation and FEM simulation.

2. Experimental

The polycrystalline Ti$_3$AlC$_2$ used in this work was prepared by in situ hot-pressing and solid–liquid reaction method as described elsewhere.[2] About 70 rectangular bars with

Table 1
The basic properties of Ti$_3$AlC$_2$ tested in this work

Properties	Value
Density	
Theoretical (g/cm^3)	4.247
Measured (g/cm^3)	4.21
Coefficient of thermal expansion (K^{-1})	9.0×10^{-6}
Electrical conductivity (Ω^{-1} m^{-1})	3.48×10^6
Temperature coefficient of resistivity (K^{-1})	0.0035
Vickers hardness (GPa)	2.7–3.2
Young's modulus (GPa)	290
Compressive strength at RT (MPa)	760
Compressive strength at 1200 °C (MPa)	195
Bending strength (MPa)	340
Brittle-to-ductile transition temperature (°C)	1050
Fracture toughness (MPa m$^{1/2}$)	6.9–7.2

the dimension of 3 mm × 4 mm × 36 mm were electrical discharge machined from an as-prepared slab of 150 mm in diameter and 25 mm in height which allows a large number of samples prepared from the same slab for an identity of the properties. All samples were polished ultimately by 0.5 μm diamond paste and chamfered on the tensile surface, and divided into 20 groups for tests at different quenching temperatures and media. The basic physical properties of the testing material are displayed in Table 1.

Thermal shock experiments were performed by quenching the Ti$_3$AlC$_2$ bars from various temperatures into 20 °C water, air and silicon oil, respectively, for comparing the thermal shock damage in different media (the emphasis was put on the quenching in water and air, only two groups of sample were quenched in oil). The samples of each group were mounted on a rectangular refractory slab, parallel and separate each other, then the slab was placed into the furnace so that at the testing temperature the samples can be simultaneously fallen into a bucket full of water or oil (20 °C and 20 l in volume and refreshed before each quenching test) placed under the furnace. The specimens were heated in air with a heating rate of 10 °C/min up to the testing temperature and were held for 20 min prior to the quenching. Analogically, air-quenching test was carried out by pouring the samples on a porous refractory brick (~60% porosity) at 20 °C in static air. All quenched samples were dried by wind blowing without other treatments before the tests of the retained strength.

The bending strengths of quenched and unquenched samples were measured in three-point bending with a span of 30 mm and a crosshead rate of 0.5 mm/min. The failed samples and fracture sections were examined by optical microscope and scanning electron microscope, respectively. Thermogravimetry examination was also carried out in a temperature range of 20–300 °C to identify the difference in water infiltration between the samples quenched in water and in air. Vickers hardness was measured with a load of 3 N and a dwell time of 15 s, on the polished surface of the samples.
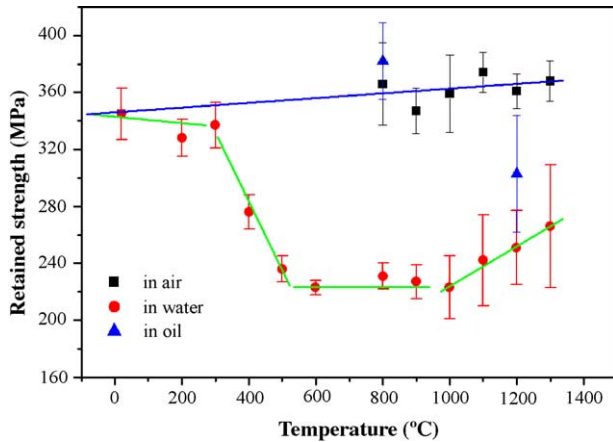
Fig. 1. Retained strength of Ti_3AlC_2 quenched in air and in water from various temperatures, showing slight reinforcing effect for samples quenched in air and four different zones for samples quenched in water.

3. Results and discussion

3.1. Retained strength and hardness

Fig. 1 compares the retained strengths of the samples quenched in air, water and oil from various quenching temperatures. For the samples quenched in air, the measured strength slightly increases rather than decreases with increasing quenching temperature, which indicates that the thermal shock by air does not yield damage in Ti_3AlC_2. On the other hand, the residual strength of the samples quenched in water exhibits a complex evolution with the increase of quenching temperature from 20 to 1300 °C, i.e., steady strength → gradual degradation → stable low retained strength → increased strength. Such a varying trend of residual strength not only confirms the abnormal strength enhancement in a temperature range[1,4] but provides more detailed damage evolution related to quenching temperature. Thus, the retained strength includes approximately four zones according to the variation of the quenching temperature: (i) no damage zone (20–300 °C), (ii) strength degradation zone (300–500 °C), (iii) stable low-strength zone (500–1000 °C), and (iv) strength enhancement zone (1000–1300 °C). Based on these results, the thermal shock resistance of Ti_3AlC_2 is estimated to be 300–400 °C, which is higher than the prediction (~107 °C) from Eq. (1), and also higher than that of alumina ($R = 100$–250 °C).[14,15] Whereas for the samples quenched in oil, the critical temperature for strength degradation is much higher than that of the samples quenched in water. Above results indicate that the rank of the cooling rates among the three quenching media is: $V_{water} > V_{oil} > V_{air}$.

In water quenching tests, unlike brittle ceramics whose strength rapidly drops at the critical temperature,[19] the strength degradation of Ti_3AlC_2 is a gradual process in the second temperature range. And the stable retained strength in the third temperature zone indicates that the increase of the temperature-drop does not lead to further damage. It is

more interesting that, when the quenching temperature is higher than 1000 °C, the retained strength increases with the increase of the quenching temperature. Therefore, the minimum retained strength, which is higher than 60% of the initial strength, is obtained in the third temperature zone. The abnormal evolution in the retained strength provides a prediction that the quantities of strength degradation caused by thermal shock should less than 40% for Ti_3AlC_2, whatever temperature difference is utilized.

Fig. 2 displays the measured hardness of the quenched samples with the increasing temperature-drop. The hardness values varying from 2.8 to 6.8 GPa show similar enhancing trend for the samples quenched in water and in air, although the retained strengths are different. In bending tests, the samples quenched in air displayed a brittle fracture mode, i.e., high strength and fast crack rate; whereas the samples quenched in water showed quasi-plastic fracture without separating into pieces after failure, i.e., relatively low-strength and low-cracking rate due to "damp" grain boundary. The terms "damp" and "dry" grain boundaries were first used by Wiederhorn to describe grains that were covered with a glassy phase or free of a second phase, respectively, in analyzing the creep resistance of ceramics.[19] In our present work, real damp grain boundaries were found from the samples quenched in water, and it made the sample not so brittle. Fig. 3 shows optical micrographs of the typical quasi-plastic fracture of a water-quenched sample in three-point bending test. Although great crack opening displacement can be seen in the tensile surface (Fig. 3a) and in the side surface (Fig. 3b), the sample is not completely fractured and no visible crack appears on the compressive surface of the bending beam (Fig. 3c). The quasi-plastic failure mode and strength degradation of the samples quenched in water indicates that the grain boundaries in the surface layer become "damp" after quenching in water. The damp grain boundary leads to a quasi-plastic fracture involving crack deflection, branching and bridging (as shown in Fig. 4a), pulling-out of grains (as shown in Fig. 4b) and degradation of grain boundary strength.
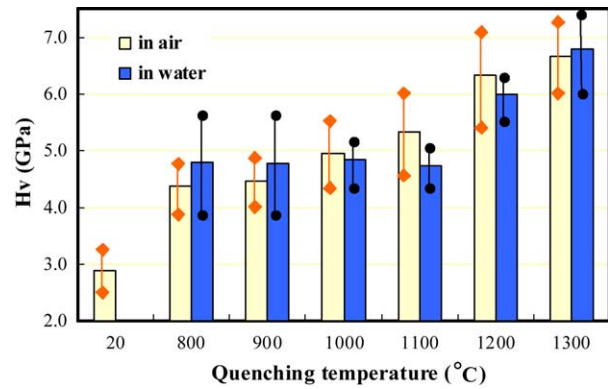

Fig. 2. Vickers hardness as a function of quenching temperature, with 3 N load and 15 s dwell time. Each value represents an average of five measurements.
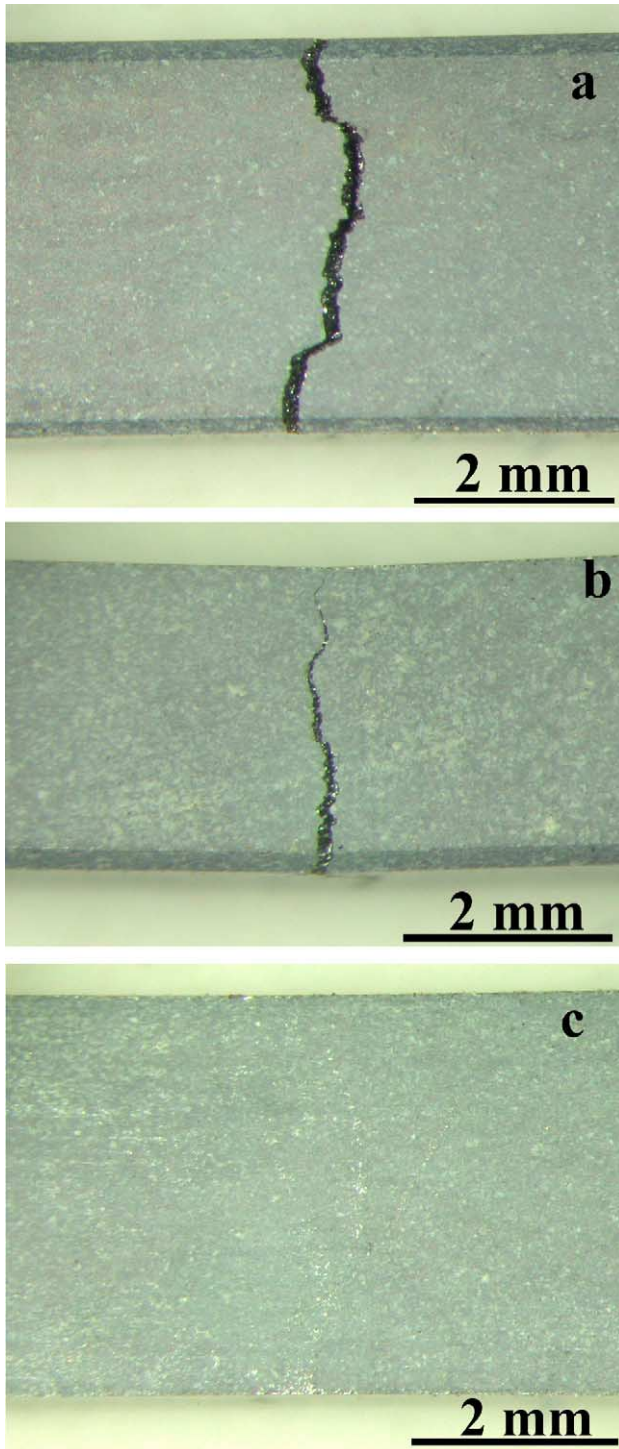
Fig. 3. Profiles of fracture sample which was quenched in water from 1000 °C before the three-point bending test. Crack opening viewed from: (a) the tensile surface of the sample, (b) the side view of the crack, and (c) the profile of the compressive surface.

3.2. Influence of water infiltration

SEM examinations on the fracture section of the samples quenched in air (Fig. 5a) and in water (Fig. 5b) show similar morphologies from which the delamination in grains,
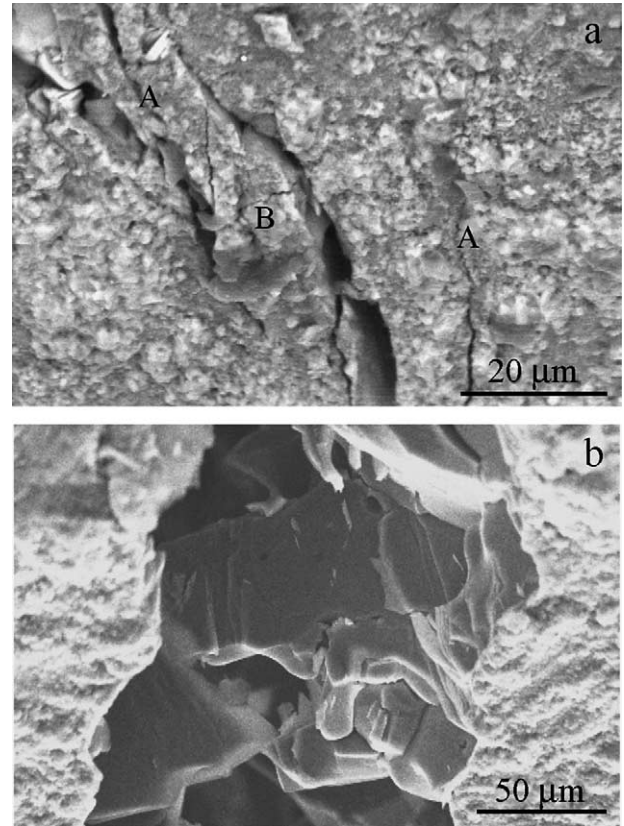

Fig. 4. Profiles of ductile fracture of the quenched sample from 1000 °C to water, showing (a) crack branch marked as A and crack bridge marked as B, and (b) grain pull-out in the crack.

transgranular and intergranular fracture can be clearly observed. The degradation of the retained strength as shown in Fig. 1 demonstrates that there must be damage in the Ti_3AlC_2 quenched in water. However, no surface cracks representing thermal shock damage were found in the careful SEM examination. A notable evidence, showing the difference in the damage mechanism between air-quenched and water-quenched samples, was found from the morphologies of grain boundaries by SEM examination, i.e., the grain boundaries of the samples quenched in water were weaker than those quenched in air. The weak grain boundaries can be clearly seen from Figs. 6 and 7, which imply that the weakening of grain boundaries leads to the quasi-plastic fracture behavior and the strength degradation of the samples quenched in water.

The weak grain boundary in the outer layer of the quenched samples is imputed to water infiltration at the moment of quenching in water. Since the layered platelet grains have anisotropic thermal expansion coefficient, the platelet grains in the surface layer suddenly shrink in different levels along different directions when the samples drop into water. Untight grain boundaries were yielded at that moment and the water would penetrate inside, which is a cause for damp grain boundaries in the water-quenched samples. Further evidence of the water infiltration was obtained by thermo-
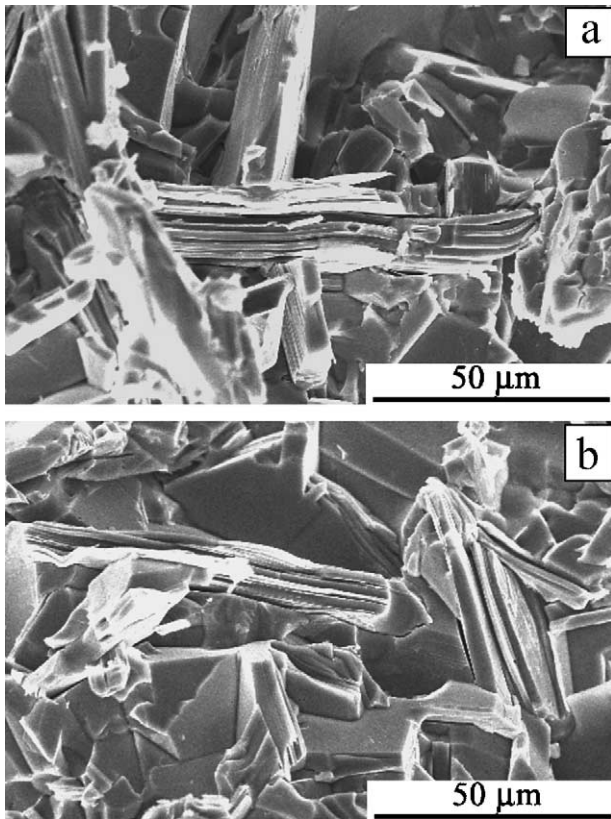
Fig. 5. SEM fractographies of quenched sample in water (a), and in air (b) from 1000 °C, showing a combination of transgranular and intergranular fracture, and also delamination in grain.

gravimetry analysis (16/18 SETARAM, France) on both samples quenched in air and in water for comparing the weight loss during heating from 20 to 300 °C under identical testing conditions. Weight loss in the sample quenched in water was obviously larger than that of air-quenched sample due to evaporation of the water in the sample. The measured difference in the weight loss between them increased with increasing temperature up to 300 °C and became stable when the relative weight loss was ∼0.0018 mg/cm^2.
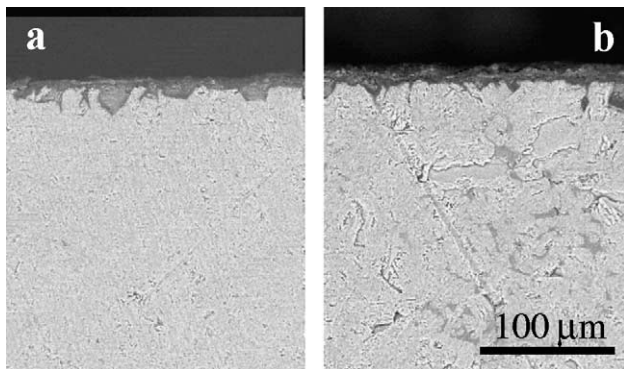

Fig. 6. SEM micrographs of Ti$_3$AlC$_2$ samples quenched from 1200 °C in air (a) and in water (b), after polishing off one oxide layer, showing similar oxide thickness but different grain boundary damage.
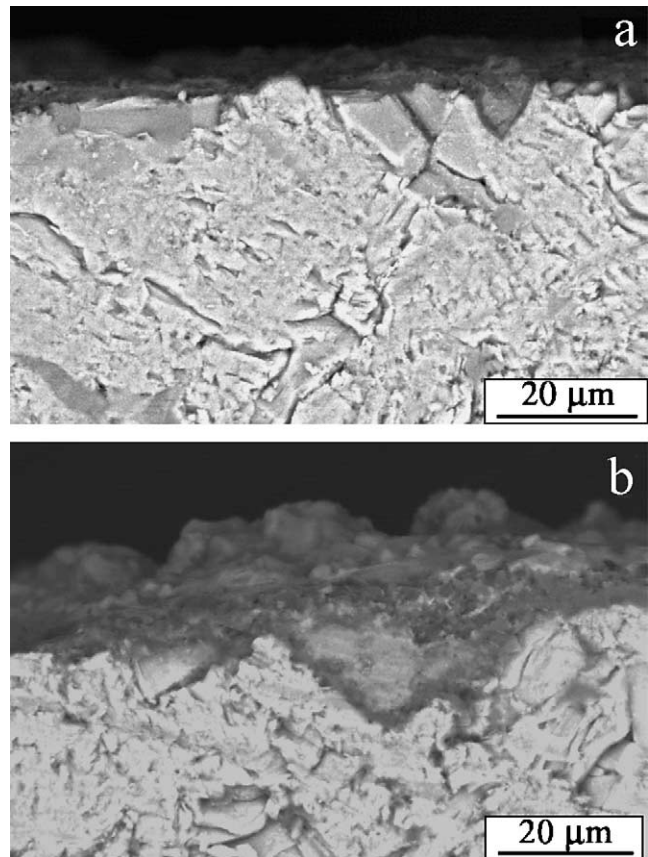

Fig. 7. The thickness of the oxide scales varying with temperature and the morphology of the polished surface showing lax grain boundary from: (a) 1000 °C to (b) 1300 °C in water.

3.3. Effects of oxidation and residual stress

The fact that the surface hardness of the quenched samples increases with the quenching temperature indicates that a hard oxide scale is generated during the heating process of the samples. Similar oxide thickness on the samples quenched in air (Fig. 6a) and in water (Fig. 6b) implies that the oxidation is formed before quenching, so it is independent of the quenching media. The thickness of the oxide scale growing with the increase of temperature confirms the prediction from kinetic study.[20] SEM micrographs (Fig. 7) show the increasing oxide thickness with the temperature and the weak grain boundary in the sample quenched in water. The oxide production of Ti$_3$AlC$_2$ is α-Al$_2$O$_3$ and the oxidation mechanism has been described elsewhere.[20,21] The oxidation results in a hard surface layer of α-Al$_2$O$_3$ on the Ti$_3$AlC$_2$ substrate; therefore, the hardness enhancement with the increasing quenching temperature is attributed to the growth of the oxide layer. The complex change of the retained strength with the quenching temperature is also related to the oxide layer.

Because of the difference between the thermal expansion coefficient of the oxide layer ($\alpha_1 = 8.3 \times 10^{-6}$ K^{-1} for α-Al$_2$O$_3$) and the substrate ($\alpha_2 = 9 \times 10^{-6}$ K^{-1} for Ti$_3$AlC$_2$), the thermal stresses will be generated in the oxide scale and

the substrate. When the thermal expansion coefficient of the outer layer is lower than that of the substrate, compressive stress will be yielded in the outer layer during cooling. It is the compressive stress in the oxide layer that improves the retained strength and damage resistance of the quenched sample. The compressive pre-stress in the oxide layer and the shear stress at the interface were calculated based on an uneven strain model.[22] For a rectangular sandwich bar sample without applied stress, the residual stress distribution along the longitudinal direction is given by:[22]

$$\tau = \frac{(n+2)\Delta T(\Delta\alpha)E_1E_2h_1h_2}{L(2E_1h_1+E_2h_2)}\xi^n = \tau_o\xi^n \qquad (2)$$

and

$$\sigma_1 = -\frac{(n+2)\Delta T(\Delta\alpha)E_1E_2h_2}{(n+1)(2E_1h_1+E_2h_2)}(1-\xi^{n+1}) \qquad (3)$$

where $\xi = x/L$ is a non-dimensional variable in the range of 0–1, τ is the shear stress at the interface, σ_1 is the compressive stress in the outer layer, L is the half length of the bar sample, h_1 is the thickness of the oxide layer, h_2 is the thickness of the substrate, $\Delta\alpha$ is the difference in the thermal expansion coefficients between the coating and substrate, τ_o is the maximum interfacial shear stress at the ends of the bar, n is a constant depending on material properties, usually 7–10 for ceramic laminates.[22]

To understand the stress distribution and stress variation with the thickness of the oxide scale, a calculation of thermal stress was carried out using the following parameters: $\Delta T = 1000\,^\circ\text{C}$, $\Delta\alpha = 0.7 \times 10^{-6}\,\text{K}^{-1}$, $h_2 = 3\,\text{mm}$, $E_1 = 330\,\text{GPa}$ ($\alpha\text{-Al}_2\text{O}_3$), $E_2 = 290\,\text{GPa}$ (Ti_3AlC_2), $n = 8$. The calculated stress distribution along the length direction of the bar (with $h_1 = 0.1\,\text{mm}$) is displayed in Fig. 8a, which indicates that the maximum compressive stress occurs at the middle of the bar and the maximum interfacial shear stress occurs at the ends of the bar. The maximum stresses varying with the thickness of the outer layer are calculated and are shown in Fig. 8b, which demonstrates that the residual stress in the outer layer slightly declines but the interfacial shear stress increases with increasing thickness ratio h_1/h_2 for a fixed temperature-drop. Since the thickness of the oxide layer increases with the quenching temperature, the residual stress in the oxide layer and the shear stress at interface also increase with the temperature. The shear stresses increasing with the thickness ratio may result in debonding and flaking away of the oxide scales when the oxide layer is too thick.

For a sample with residual stress, a common failure criterion is that fracture occurs when the sum of the applied stress and the residual stress exceeds the strength of the material. The location of the fracture initiation depends on the competition between the stress sum in the coating and in the substrate. Thus, the enhancement of the flexure strength resulted from the oxide layer involves two cases: (i) when fracture initiates from the oxide layer, the strength of the coated sample would increase with increasing compressive pre-stress in the outer layer and (ii) if fracture initiates from the substrate, the
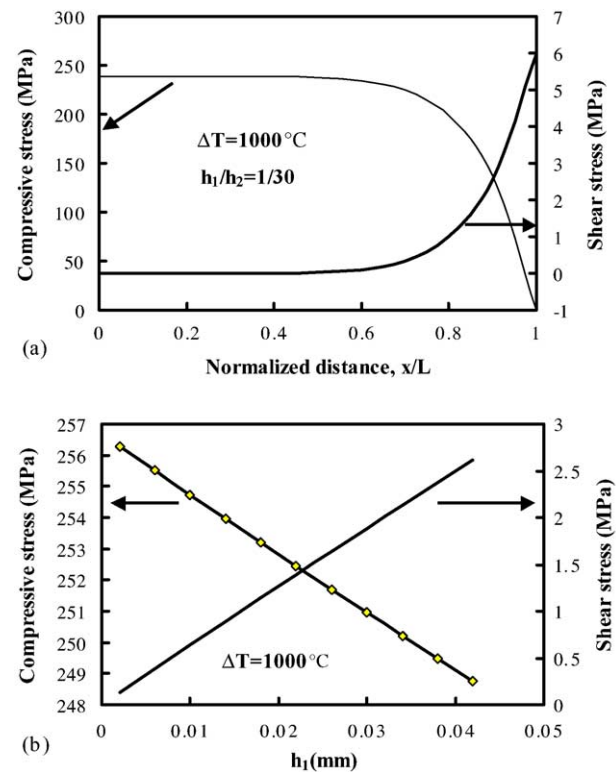

Fig. 8. (a) Calculated retained stresses in the oxide layer and the interfacial shear stresses distributing along half-length of the sample, for $\Delta T = 1000\,^\circ\text{C}$, $\Delta\alpha = 0.7 \times 10^{-6}\,\text{K}^{-1}$, $h_1 = 0.01\,\text{mm}$, $h_2 = 3\,\text{mm}$, $E_1 = 330\,\text{GPa}$, $E_2 = 290\,\text{GPa}$, $n = 8$. The middle and the end of the bar corresponds to $x = 0$ and $x = L$, respectively. (b) Influence of the thickness of the oxide scale on the maximum residual stress and maximum shear stress, calculated by the uneven strain model for $h_2 = 3\,\text{mm}$.

flexure strength of the sample would increase with increasing thickness of the outer layer. In both cases, therefore, the retained strength would increase with increasing temperature because the compressive pre-stress in the oxide layer and the thickness of the oxide layer increase with temperature, in the range of 1000–1300 °C. Obviously, the prerequisite for this strength enhancement is that no damage is generated in the oxide layer. Although low thermal shock resistance was often reported for Al_2O_3,[14,15] no crack is found on the oxide layer formed on Ti_3AlC_2 by SEM observation. The fact that the Al_2O_3 coating is not damaged up to 1300 °C quenching is due to the thickness effect[15] (the layer was very thin), the excellent thermal conductivity of both Ti_3AlC_2 and $\alpha\text{-Al}_2\text{O}_3$, and the compressive pre-stresses in the layer. In the third temperature zone, the stable retained strength of the samples quenched in water implies a balance between the strength degradation and strength increase relating to different mechanisms.

The effects of the oxide scale on strength are also confirmed by a failure simulation in three-point bending using finite element method (FEM). Stress calculation was performed with 40,000 meshes in plane strain under an initial load (stress or displacement), and then the stress in every element is examined with the modified Mohr–Coulomb failure
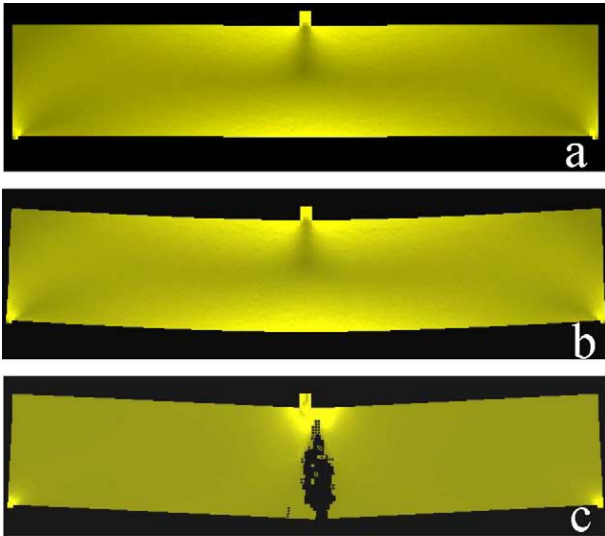
Fig. 9. Results of FEM simulation on the failure of monolithic beam at increasing three-point bending loads step by step at: (a) 50 MPa; (b) 250 MPa; and (c) 252 MPa. The initial modulus and strength for the simulation were 280 GPa and 260 MPa, respectively.

criterion to control the failure of each element. The same calculation and examination are repeated after a load increment (0.001 mm in deflection increment), step by step until fracture occurs in the sample. To compare the failure stress between a monolithic beam and coated beam, identical sample sizes and loading conditions were used to simulate the failure. Figs. 9 and 10 show respectively the failure process and critical stress to fracture in the monolithic sample and coated sample. It indicates that the bending strength of the sample with a 0.01 mm thick alumina coating is about 5–10% higher
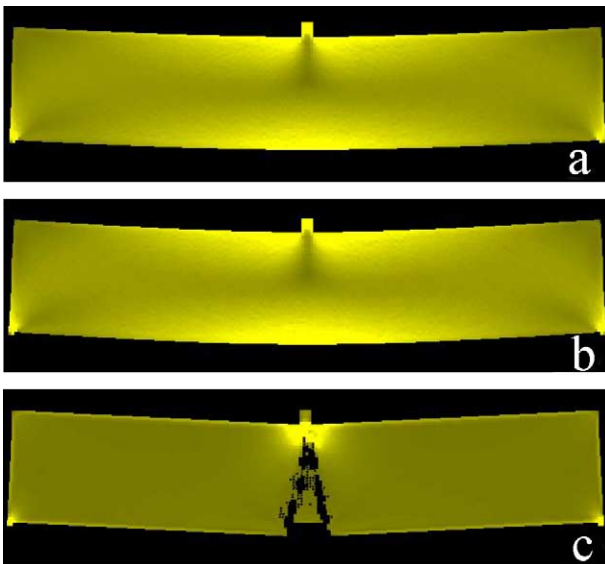

Fig. 10. Results of FEM simulation on three-point bending failure of coated sample with the same initial parameters as in Fig. 9 at: (a) 200 MPa; (b) 266 MPa; and (c) 270 MPa. Initial modulus and strength of coating were 300 GPa and 280 MPa, $\Delta\alpha\Delta T = 0.007$.

than the monolithic Ti_3AlC_2 sample because of the residual stresses.

4. Conclusions

(1) Quenching in air does not result in damage in the layered machinable Ti_3AlC_2 ceramic, no strength degradation but somewhat strength enhancement is found for the air-quenched samples up to the quenching temperature of 1300 °C.

(2) Thermal shock resistance of Ti_3AlC_2 quenched in water is 300–400 °C, and the quenched samples exhibit quasi-plastic fracture mode in bending tests. The retained strength shows different variations in four zones of quenching temperature: (i) below 300 °C, no strength loss; (ii) 300–500 °C, strength degradation; (iii) 500–1000 °C, stable low-strength; and (iv) 1000–1300 °C, strength increases with increasing temperature difference. This abnormal thermal shock behavior indicates that strength loss in Ti_3AlC_2 caused by thermal shock should be less than 40% in any case.

(3) The samples quenched in silicon oil from 800 °C show similar results as quenching in air, but quenching from 1200 °C to oil leads to a strength degradation. Therefore, the cooling rates for the three quenching media are ranked as: $V_{water} > V_{oil} > V_{air}$.

(4) The strength degradation and quasi-plastic fracture of the samples quenched in water is imputed to weakening of grain boundaries caused by water infiltration. Whereas strength enhancement of the samples quenched from the temperatures above 1000 °C into water is attributed to (i) growth of oxide scale (α-Al_2O_3) with increasing temperature and (ii) the residual compressive stress in the scale, which is irrelevant of the thermal shock.

(5) The measured hardness of the samples quenched in water and in air shows similar values and identical dependence on temperature difference. The hardness increases with increasing quenching temperature due to the formation of hard α-Al_2O_3 layer.

(6) The stress analysis reveals that the maximum compressive stress in the oxide layer occurs at the middle of the bar, and the maximum interfacial shear stress occurs at the ends of the bar. Strength enhancement for coated sample is confirmed by FEM failure simulation when the expansion coefficient of the coating is lower than that of the matrix.

References

1. Tzenov, N. V. and Barsoum, M. W., Synthesis and characterization of Ti_3AlC_2. *J. Am. Ceram. Soc.*, 2000, **83**, 825–832.

2. Wang, X. H. and Zhou, Y. C., Solid–liquid reaction synthesis of layered machinable Ti_3AlC_2 ceramic. *J. Mater. Chem.*, 2002, **12**, 455–460.

3. Lopacinski, M., Puszynski, J. and Lis, J., Synthesis of titanium aluminum carbides using self-propagating high-temperature synthesis technique. *J. Am. Ceram. Soc.*, 2001, **84**, 3051–3053.

4. Wang, X. H. and Zhou, Y. C., Microstructure and properties of Ti_3AlC_2 prepared by the solid–liquid reaction synthesis and simultaneous in-situ hot pressing process. *Acta Mater.*, 2002, **50**, 3141–3149.

5. Myhra, S., Crossley, J. A. A. and Barsoum, M. W., Crystal-chemistry of the Ti_3AlC_2 and Ti_4AlN_3 layered carbide/nitride phases-characterization by XPS. *J. Phys. Chem. Solids*, 2001, **62**, 811–817.

6. Zhou, Y. C. and Wang, X. H., Electronic and structural properties of the layered ternary carbide Ti_3AlC_2. *J. Mater. Chem.*, 2001, **11**, 2335–2339.

7. Low, I. M., Lee, S. K., Lawn, B. R. and Barsoum, M. W., Contact damage accumulation in Ti_3SiC_2. *J. Am. Ceram. Soc.*, 1998, **81**, 225–228.

8. Bao, Y. W., Chen, J. X., Wang, X. H. and Zhou, Y. C., Shear strength and shear failure of layered machinable Ti_3AlC_2 ceramics. *J. Eur. Ceram. Soc.*, 2004, **24**, 855–860.

9. Hasselman, D. P. H., Thermal stress resistance parameters for brittle refractory ceramics: a compendium. *Am. Ceram. Soc. Bull.*, 1970, **49**, 1033–1037.

10. Pettersson, P., Johnsson, M. and Shen, Z., Parameters for measuring the thermal shock of ceramic materials with an indentation-quench method. *J. Eur. Ceram. Soc.*, 2002, **22**, 1883–1889.

11. Faber, K. T., Huang, M. D. and Evans, A. G., Quantitative studies of thermal shock in ceramics based on a novel test technique. *J. Am. Ceram. Soc.*, 1981, **64**, 296–300.

12. Collin, M. and Rowcliffe, D., Analysis and prediction of thermal shock in brittle materials. *Acta Mater.*, 2000, **48**, 1655–1665.

13. Bao, Y. W. and Jin, Z. Z., Size effects and a mean-strength criterion for ceramics. *J. Fatigue Fract. Eng. Mat. Struct.*, 1993, **16**, 829–833.

14. Kim, I. S., Thermal shock resistance of the Al_2O_3-metal composites made by reactive infiltration of Al into oxide fiber board. *Mat. Res. Bull.*, 1998, **33**, 1069–1075.

15. Sherman, D. and Schlumm, D., Thickness effect in thermal shock of alumina ceramics. *Scr. Mater.*, 2000, **42**, 819–825.

16. Anderson, T. and Rowcliffe, D. J., Indentation thermal shock test for ceramics. *J. Am. Ceram. Soc.*, 1996, **79**, 1509–1514.

17. Pettersson, P., Shen, Z., Johnsson, M. and Nygren, M., Thermal shock resistance of α/β-sialon ceramic composites. *J. Eur. Ceram. Soc.*, 2001, **21**, 999–1005.

18. Hirano, T. and Niihara, K., Thermal shock resistance of Si_3N_4/SiC nanocomposites fabricated from amorphous Si–C–N precursor powers. *Mater. Lett.*, 1996, **26**, 285–289.

19. Wiederhorn, S. M., Hockey, B. J. and French, J. D., Mechanism of deformation of silicon nitride and silicon carbide at high temperatures. *J. Eur. Ceram. Soc.*, 1999, **19**, 2273–2284, doi:10.1016/S0955-2219(99)00121-1.

20. Wang, X. H. and Zhou, Y. C., Oxidation behavior of Ti_3AlC_2 at 1000–1400 °C in air. *Corrosion Sci.*, 2003, **45**, 891–907.

21. Wang, X. H. and Zhou, Y. C., Oxidation behavior of Ti_3AlC_2 powders in flowing air. *J. Mater. Chem.*, 2002, **12**, 2781–2785.

22. Bao, Y. W., Su, S. B. and Huang, J. L., An uneven strain model for analysis of residual stress and interface stress in laminated composites. *J. Composit. Mater.*, 2002, **36**, 1769–1778.